Supporting Information

Ganesan and Boxer 10.1073/pnas.0901770106

SI Text

Substrate Fabrication Process. Fig. S1 shows the stages of fabrication of the well (described in *Materials and Methods*).

Bilayer Formation in Greater Detail. Figs. S2 and S3 give more detail about the postulated bilayer formation process and what was observed experimentally.

Fig. S2 shows the 4 major stages of bilayer formation. First, 20 μl decane is dispensed on the chip with a micropipettor in the presence of aqueous carboxyfluorescein (CF). The decane is spread but remains a thick, macroscopically visible droplet initially covering a substantial ($>$ 50%) fraction of the chip. After washing the bulk solution, fluorescence from CF trapped in small aqueous volumes in the wells can be seen (Fig. S2*A*).

Next, phospholipid vesicles are added to the bulk (upper) aqueous layer and the system left to stand for 8–15 h (Fig. S2*B*). During this time, some of the vesicles dissolve into the decane film, and lipid monolayers would be expected to form at the decane/water interfaces (Fig. S2*C*). Presumably due to the resulting change in interfacial energy, the visible decane droplet thins and contracts until it is in a small area on the chip. For some wells the monolayers come together to form lipid bilayers (Fig. S2*D*). These wells are concentrated just outside of the edges of the remaining decane droplet. This process occurs spontaneously or can be induced in wells near the decane edge by physically spreading the thick decane film with a small air bubble. By the time of imaging, most wells have no lipid spread across them (as evidenced by loss of trapped carboxyfluorescein dye). Typically these wells are far from the remaining decane bead, and, presumably, as the film over these wells thinned and receded, it was ruptured by washing steps or because of inherent instability. Those wells under the remaining decane bead have a thick film of decane rather than a bilayer spanning them. Typically only wells near the edge of the decane bead form bilayer or "black" lipid membranes (BLMs) that can be imaged on the microscope.

Fig. S3 shows 2 experimental observations of spontaneous decane film recession observed in the DiI fluorescence signal. In both cases, wells were observed close to a decane film edge but still covered by the film. Note that, because the film is of nonuniform thickness near its edge, it has bright and dark fringes of fluorescence because of interference from the reflective gold surface affecting the monolayer at the water/decane interface (where the phospholipids and fluorophores are expected to concentrate). Rings of bright and dark fluorescence in the wells can also be observed in Fig. S3 *A* and *C*, superimposed over the linear fringes. The rings can be attributed to interference affecting the monolayer at the lower water/decane interface. After film recession, only the rings (consistent with a curved bilayer) are visible (Fig. S3 *B* and *D*).

Fig. S2 also illustrates aspects of our model for BLM formation on the platform we have described. An expected contact angle θ_{calc} of decane on the gold self-assembled monolayer (SAM) under water was calculated by starting with the Young equation:

$$\gamma_{SAM/decane} + \gamma_{decane/water}\cos(\theta_{calc}) = \gamma_{SAM/water}. \quad [1]$$

To determine an expected value, we used the contact angles of water and decane on the gold SAM in air:

$$\gamma_{SAM/decane} + \gamma_{decane}\cos(\theta_{decane}) = \gamma_{SAM} \quad [2]$$

$$\gamma_{SAM/water} + \gamma_{water}\cos(\theta_{water}) = \gamma_{SAM} \quad [3]$$

Equating Eq. **S2** and Eq. **S3** yields:

$$\gamma_{decane}\cos(\theta_{decane}) - \gamma_{water}\cos(\theta_{water}) = \gamma_{SAM/water} - \gamma_{SAM/decane} \quad [4]$$

Combining Eq. **S4** with Eq. **S1** gives:

$$\gamma_{decane}\cos(\theta_{decane}) - \gamma_{water}\cos(\theta_{water}) = \gamma_{decane/water}\cos(\theta_{calc}). \quad [5]$$

We measured contact angles on a gold SAM on an unpatterned substrate (i.e., no topographical features or exposed SiO_2). Our measurements of θ_{water} and θ_{decane} were 105° and ≈30°, respectively. These correspond well enough with literature values (1) for the purposes of the rough calculation we were performing. Using values for the surface energies and interfacial tensions from Israelachvili (2) (p315) for water, octane, and octane/water of 72, 22, and 51 mJ/m^2, we calculate θ_{calc} = 42°.

This calculation is borne out by our observations of decane in water on a gold SAM. The decane spreads on the gold to form a discrete droplet with a curved upper water/decane interface. One would expect that the lower water/decane interfaces (in individual wells) would form a similar contact angle on gold, as represented in Fig. S2 *A* and *B*.

Applying the same contact angle theory as before (Eq. **S5**) for the PEG-silane SiO_2 surface, with water having a contact angle in air of ≈40°, leads to the conclusion that decane should have a large (>90°) contact angle with the SiO_2 under water. Thus, if the decane came in contact with the SiO_2 surface on the well side wall, the concavity of the interface would change, and it would be quite plausible that the decane would make contact with the SiO_2 well bottom. Because we do not see this in successful bilayer experiments, we conclude that the decane does not spread onto the SiO_2 surface.

We cannot measure the precise details of the curvature of the lower interface. Qualitatively, it seems unlikely that the interface is spherically curved at a 42° contact angle because this would lead to the interface extending by ≈4 μm above the substrate surface for a 20-μm diameter well. It is possible there is an equilibrium between the energy gained from thickening of decane at a more curved interface in the edge region of the well and the work required to displace higher density water from this region. Another factor to consider is the likelihood of topographic defects in the wells' side walls arising from fabrication processes such as the reactive ion etch. These may produce interface behavior very different from assumptions derived from analysis of bulk surface properties.

The addition of lipid vesicles and their gradual transfer into the decane layer causes substantial changes in the decane, notably thinning and "beading up," i.e., a substantial decrease in the contact angle of the water/decane/gold SAM system. This seems likely to be primarily due to a decrease in $\gamma_{water/decane}$ rather than the effect on γ_{water} or γ_{decane}. We commonly observed that wells far from the remaining bead of decane/lipid do not support bilayers or contain CF dye, suggesting rupture of the decane film over the wells as it thinned. The observation suggests that films that thin the soonest after lipid addition are unstable and rupture. This could be occurring because of incomplete adsorption of lipids at the interfaces when the decane in those areas of the chip thinned, i.e., the interface properties were intermediate between the conditions that lead to a stable decane droplet and those that support bilayer formation. Bilayers were

usually observed near the edges of the residual decane/lipid bead, where, presumably, well-packed lipid monolayers had formed at the interfaces.

Fluorescence Characterization of Bilayers. For Co^{2+} quenching (3), 0.33 M $CoCl_2$ in 10 mM MOPS pH 7.2 was added to the bulk aqueous layer of a standard bilayer preparation, diluting the solution to a final concentration of ≈80 mM Co^{2+} and ≈0.38 M Na^+. The fluorescence signals of the dyes in the system were monitored as the Co^{2+} was washed out with 0.50 M NaCl in 10 mM MOPS. The heavy-atom quencher reversibly quenched 100% of Cy5-DNA fluorescence and 50% of DiI fluorescence (Fig. S4*A*). The fluorescence of trapped CF was not quenched by Co^{2+} addition, even though free CF was quenched at similar concentrations of Co^{2+} in fluorimeter experiments. However, CF fluorescence did decrease with increasing [Co^{2+}]. This decrease in fluorescence was attributed to an inner-filter effect caused by the high optical density of $[Co(OH_2)_6]^{2+}$ at 520 nm (the CF emission maximum).

FRAP was performed by photobleaching a spot defined by using an iris of variable radius placed in the microscope field diaphragm plane. Bleach spot sizes were typically ≈120 μm in diameter, i.e., the bleached area was much larger than the size of an individual well. Images of the recovery of fluorescence were acquired at regular intervals for a period of 20 min. The rate and extent of fluorescence recovery were determined for the entire area of the freestanding bilayer by using a single exponential fit, based on the model of Axelrod et al. (4). Typical recovery traces are shown in Fig. S4*B*. On photobleaching, both DiI and Cy5 fluorescence intensities over wells displayed >90% recovery, indicating a negligible immobile fraction for both dyes. CF trapped in the well, by contrast, was permanently bleached and did not recover. The diffusion coefficients of DiI and Cy5 were found to be approximately the same at 3.0 ± 0.8 $\mu m^2/s$ (n = 7) and 2.3 ± 0.8 $\mu m^2/s$ (n = 3), respectively. We note that fluorescence recovery rates measured for bleached lipid thin films on gold surfaces surrounding the wells had similar values. Therefore, the diffusion coefficient of lipids in the BLMs may be faster than the measured value because fluorescent lipids first have to diffuse over the bleached gold surface to reach the wells, given our large spot size, and diffusion on gold may be the rate-limiting process.

Gramicidin—Additional Experiments. Further experiments were done to demonstrate gramicidin-mediated cation transport by using the equilibrium:

$$Na^+_{(upper)} + H^+_{(lower)} \rightleftharpoons Na^+_{(lower)} + H^+_{(upper)}\ K = 1.$$

The experiment shown in Fig. S5 *A–C* demonstrates the different behavior of putative bilayers and decane thin films. Small amounts of gramicidin were added to the lipid mixture used, and bilayers were formed at pH 6.0 so that CF fluorescence was dim. Different effects were observed for bilayers and thin films when $pH_{(upper)}$ was increased to 7.2 (t = 0–4 min) and then returned to 6.0 (t = 18–20 min). Fig. S5 *A* and *B* show Cy5 fluorescence from the region examined at t = 0 and 15 min, respectively. Fig. S5*C* shows the CF fluorescence measured over the course of the experiment. For bilayers, the CF fluorescence increased by ≈70% with the 1.2 unit increase in $pH_{(upper)}$ and decreased to its original value when $pH_{(upper)}$ was returned to 6.0. In contrast, the CF fluorescence intensity in aqueous compartments trapped by decane thin films stayed relatively constant. The CF fluorescence traces of 3 individual wells that transitioned from thin films to bilayers during the experiment, marked in the Cy5 fluorescence images Fig. S5*A* (t = 0 min) and Fig. S5*B* (t = 15 min), are also shown in Fig. S5*C*. The fluorescence signals from these wells show that gramicidin-mediated change in $pH_{(lower)}$ is rapid on the formation of bilayers.

The effect of changing [$Na^+_{(upper)}$] was explored further giving the results shown in Fig. S5*D*. In this experiment, (i) $pH_{(upper)}$ was first increased from 6.0 to 7.2, (ii) [$Na^+_{(upper)}$] was decreased 10-fold to 50 mM (with the remainder of the salt replaced by $MgCl_2$), and finally (iii) [$Na^+_{(upper)}$] was entirely replaced by $MgCl_2$. The responses were as expected: (i) an increase in CF fluorescence (increase in $pH_{(lower)}$); (ii) a small decrease in fluorescence, stabilizing at an intermediate value consistent with a reduction of $pH_{(lower)}$ by ≈1 unit; and (iii) a decrease in CF fluorescence to values consistent with $pH_{(lower)} < 6.0$.

Derivation of Geometric Parameters and Relationships. Fig. S6 shows a cross-section of a spherical cap over a cylindrical well. This simplified model shows the bilayer as a circular arc; its maximum height, d_0, is at the middle of the well. At the edge of the well, distance r_{edge} from the middle, the bilayer has curved down to height d_{edge}, which should coincide with the position of the gold film relative to the well bottom. The center of the bilayer's circular arc lies on the vertical axis, distance R_c (the radius of curvature) from the bilayer. This picture, with the parameters d_0 and R_c, was used in the fluorescence interference contrast (FLIC) and variable incidence angle (VIA-FLIC) fitting models to fit the bilayer position based on interferometry data. By using this picture, further relationships between the parameters can be derived.

Relationship of d_0 and R_c. From the equation for a circle,

$$r^2_{edge} + (d_{edge} - d_0 + R_c)^2 = R_c^2$$

$$r^2_{edge} + (d_{edge} - d_0)^2 + R_c^2 + 2R_c(d_{edge} - d_0) = R_c^2$$

$$d_0 = (r^2_{edge}/2)(1/R_c) + d_{edge}.$$

In the last step, $(d_{edge} - d_0)^2$ is treated as small with respect to the other terms. This is reasonable because the value of the term is $<<1$ μm; given that R_c is ≈100 μm and r_{edge} is ≈10 μm, when squared the terms differ by at least 2 orders of magnitude. Making this assumption, the linear relationship between d_0 and $1/R_c$ is derived by geometric arguments. This relationship was verified experimentally (see *Results* and Fig. 5).

Volume Trapped by the Bilayer. The trapped volume is, to a first approximation, composed of a cylinder and a spherical cap. The volume is simply the sum of these parts:

$$V = \pi r^2_{edge} d_{edge} + \frac{1}{3}\pi(d_0 - d_{edge})^2(3R_c - (d_0 - d_{edge})).$$

For volume determinations used in Fig. 6, r_{edge} was assumed to be 10 μm, and d_0–d_{edge} (and hence d_{edge}) was determined by Pythagoras' theorem. Note that this approach does not take into account the volume of the bilayer annulus. The existence of an annulus will affect the real volume trapped in the well, whether by causing the bilayer to deviate from an ideal spherical cap shape or simply through an excluded volume effect.

1. Ron H, Rubinstein I (1994) Alkanethiol Monolayers on Preoxidized Gold. Encapsulation of Gold Oxide under an Organic Monolayer. *Langmuir* 10:4566–4573.
2. Israelachvili JN (1992) *Intermolecular and Surface Forces* (Academic, London).
3. Ajo-Franklin CM, Yoshina-Ishii C, Boxer SG (2005) Probing the structure of supported membranes and tethered oligonucleotides by fluorescence interference contrast microscopy. *Langmuir* 21:4976–4983.
4. Axelrod D, Koppel DE, Schlessinger J, Elson E, Webb WW (1976) Mobility measurement by analysis of fluorescence photobleaching recovery kinetics. *Biophys J* 16:1055–1069.

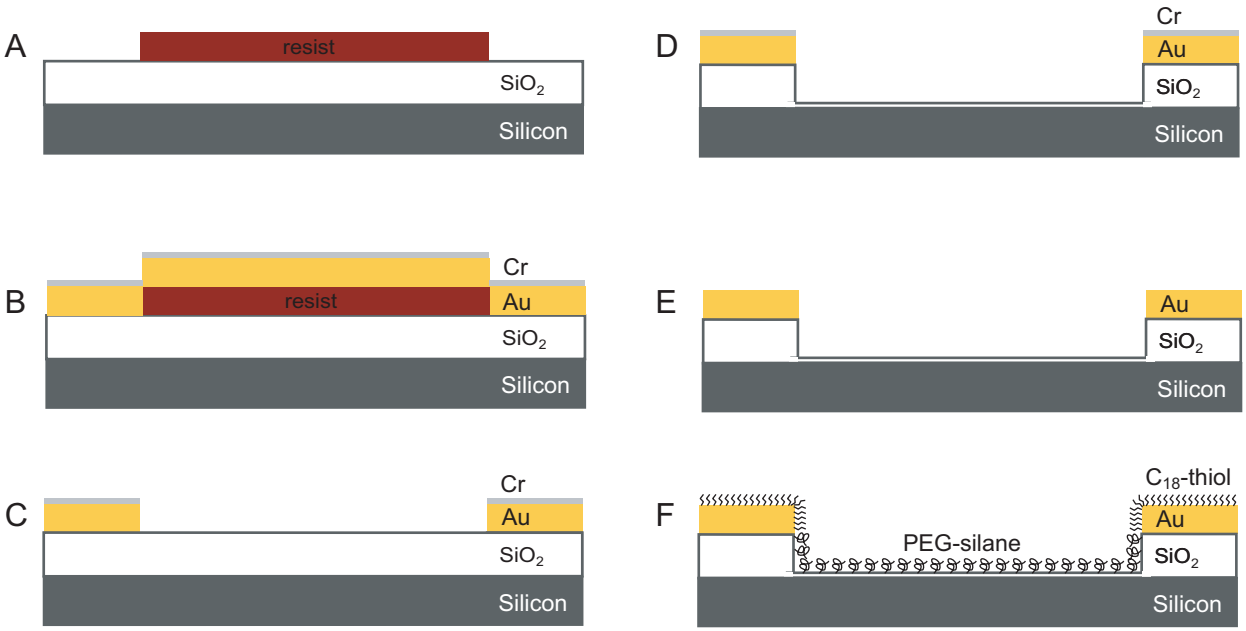

Fig. S1. Fabrication process flow for functionalized gold/silica wells on silicon. Stages A–F are described in *Materials and Methods*.

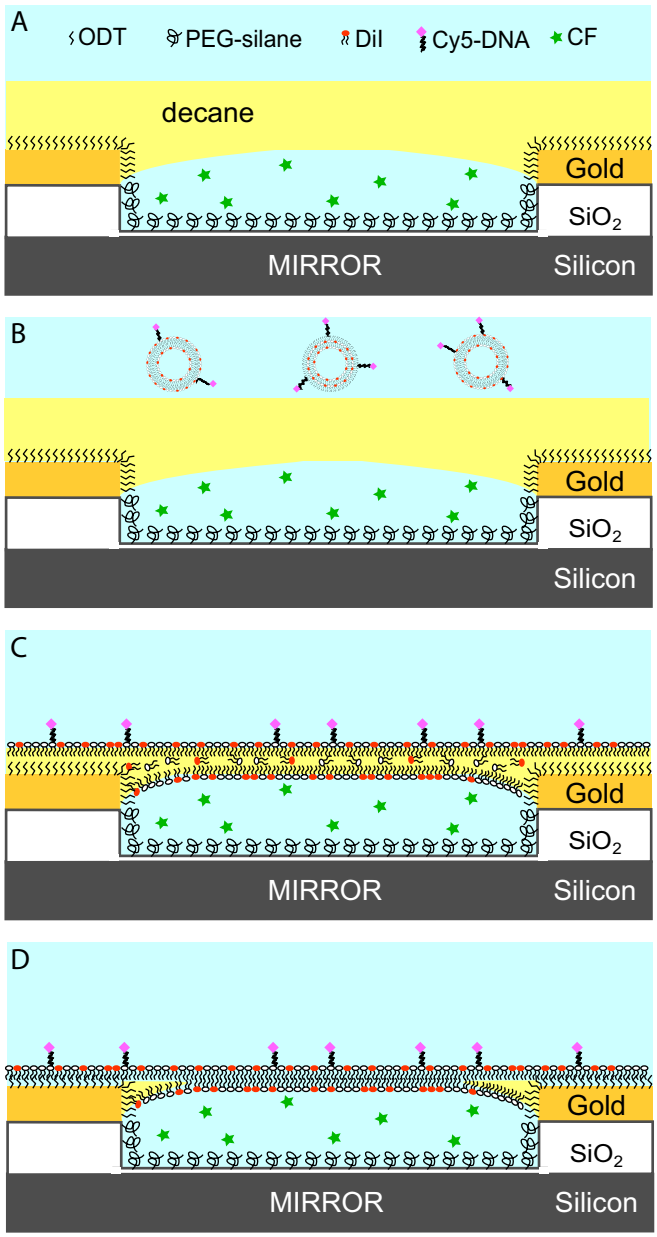

Fig. S2. Bilayer formation diagram. (*A*) A droplet of decane separates a trapped aqueous volume (containing CF) from the bulk solution. Although the upper decane/water interface is shown flat, it forms a spherical cap-shaped droplet at longer length scales. (*B*) Addition of phospholipid vesicles containing DiI, decorated with Cy5-DNA. (*C*) Vesicles dissolve into the decane and lipid monolayers form at the water/decane interfaces. (*D*) The film thins, spontaneously or with assistance, so that bilayers form.

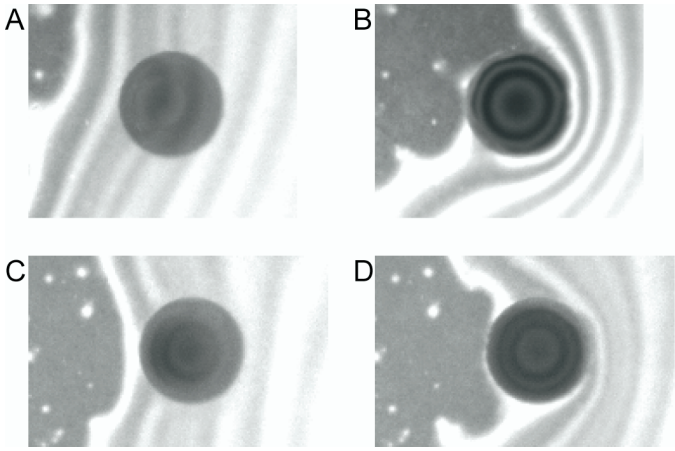

Fig. S3. Spontaneously receding decane film observed by DiI fluorescence. (*A* and *C*) Wells covered with a decane film receding to the right. (*B* and *D*) The same wells after the film edge has retreated, leaving behind fluorescent lipid with interference rings consistent with bilayer formation.

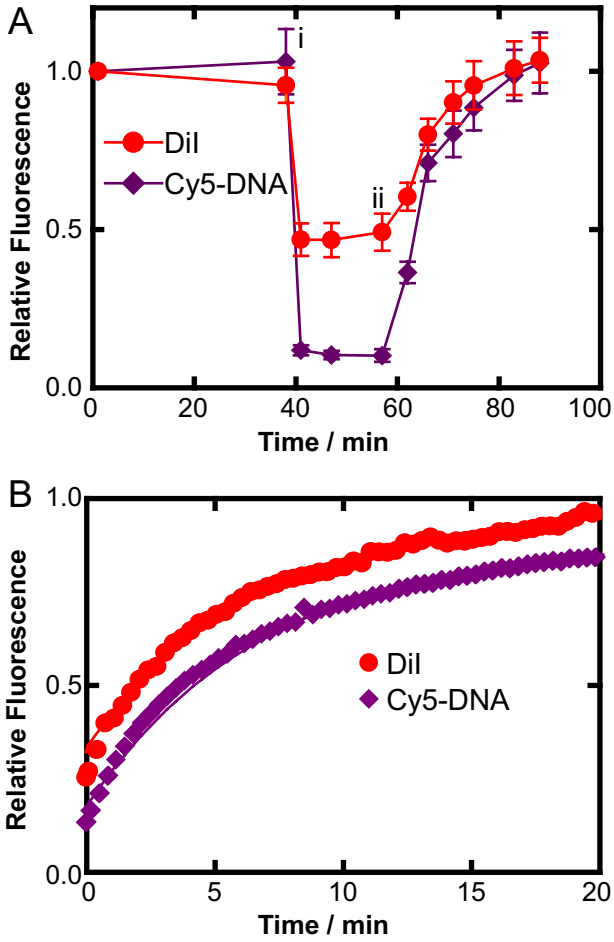

Fig. S4. Freestanding bilayer characterization. (*A*) Response of DiI and Cy5-DNA fluorescence intensity to the addition of Co^{2+} quencher (stage i) and its gradual removal by exchange (stage ii) demonstrating 50% and 100% quenching of DiI and Cy5-DNA fluorescence, respectively. (*B*) Fluorescence recovery after photobleaching profiles of DiI and Cy5-DNA. Bleach spots were ≈120 μm diameter.

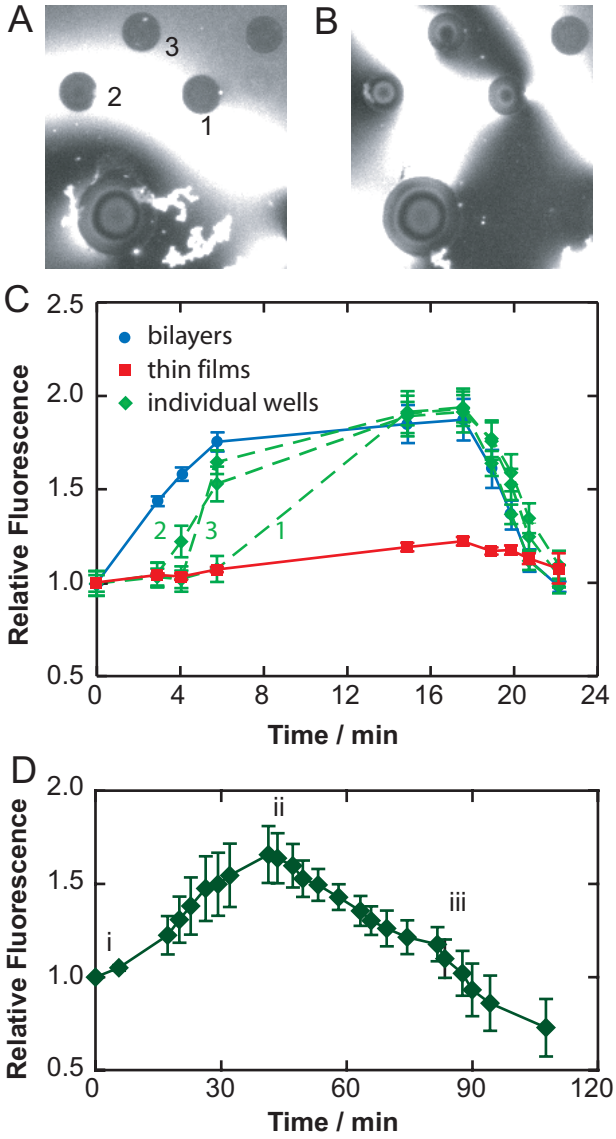

Fig. S5. Additional gramicidin experiments. (*A* and *B*) Cy5 fluorescence images of wells at a decane film edge initially (*A*) and after 15 min (*B*). Three wells, labeled 1, 2, and 3, thinned to bilayers in this time. (*C*) Response of CF fluorescence as $pH_{(upper)}$ is increased (0 min) and decreased (17 min) for bilayers (circles, $n = 5$) and thin films (squares, $n = 5$). These wells are not shown in *A* and *B*. Wells 1, 2, and 3 (diamonds) are shown separately. (*D*) CF fluorescence as i) $pH_{(upper)}$ is increased from 6.0 to 7.2; ii) Na^+ at 0.5 M is exchanged for Na^+ at 50 mM (Mg^{2+} at 0.25 M); iii) buffer is exchanged for Mg^{2+} at 0.3 M ($n = 13$).

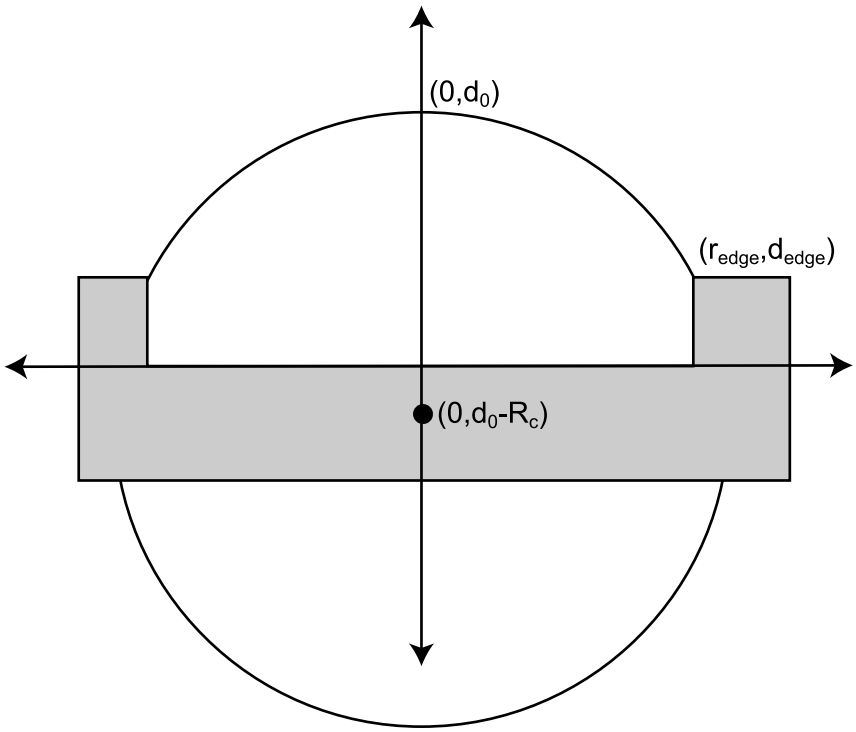

Fig. S6. Defining a coordinate system for a spherical-cap bilayer cross-section, which is a circular arc (this diagram is not to scale). The arc is centered at (0, d_0–R_c), with radius R_c and y-intercept d_0. The intersection of the bilayer and the substrate occurs at (r_{edge}, d_{edge}).